

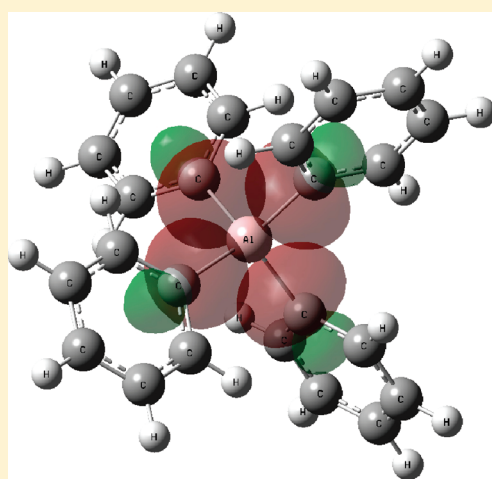
# Structural Analysis of Electrolyte Solutions for Rechargeable Mg Batteries by Stereoscopic Means and DFT Calculations

Nir Pour, Yossi Gofer, Dan T. Major, and Doron Aurbach

Department of Chemistry and the Lise Meitner-Minerva Center of Computational Quantum Chemistry, Bar-Ilan University, Ramat-Gan 52900, Israel

**S** Supporting Information

**ABSTRACT:** We present a rigorous analysis of unique, wide electrochemical window solutions for rechargeable magnesium batteries, based on aromatic ligands containing organometallic complexes. These solutions are comprised of the transmetalation reaction products of  $\text{Ph}_x\text{MgCl}_{2-x}$  and  $\text{Ph}_y\text{AlCl}_{3-y}$  in different proportions, in THF. In principle, these reactions involve the exchange of ligands between the magnesium and the aluminum based compounds, forming ionic species and neutral molecules, such as  $\text{Mg}_2\text{Cl}_3^+ \cdot 6\text{THF}$ ,  $\text{MgCl}_2 \cdot 4\text{THF}$ , and  $\text{Ph}_y\text{AlCl}_{4-y}^-$  ( $y = 0-4$ ). The identification of the equilibrium species in the solutions is carried out by a combination of Raman spectroscopy, multinuclear NMR, and single-crystal XRD analyses. The association of the spectroscopic results with explicit identifiable species is supported by spectral analyses of specially synthesized reference compounds and DFT quantum-mechanical calculations. The correlation between the identified solution equilibrium species and the electrochemical anodic stability window is investigated. This study advances both development of new nonaqueous solution chemistry and possible development of high-energy density rechargeable Mg batteries.



## INTRODUCTION

During the past decade we had been developing new classes of nonaqueous electrolyte solutions, from which metallic magnesium can be electrochemically deposited reversibly, and magnesium ions may intercalate in appropriate inorganic hosts.<sup>1,2</sup> The first electrolyte solutions presented, the DCC (“Dichloro complex”) electrolyte family, were based on the reaction products of the Lewis bases  $\text{R}_x\text{MgCl}_{2-x}$  with a variety of Lewis acids  $\text{R}'_y\text{AlCl}_{3-y}$  ( $\text{R}, \text{R}' = n$ -butyl and/or ethyl,  $x = 0-2$ ,  $y = 0-3$ ), all dissolved in THF. The equilibrium species in these solutions, which dominate its electrochemical characteristics, are the consequence of transmetalation reactions, where the organic and inorganic ligands are rapidly exchanged between the magnesium and aluminum cores.<sup>3</sup> The solvent also plays an important role in these reactions, both as a strong donor and as a polar medium that yields high ionic conductivity solutions. These electrochemical systems exhibit an electrochemical window of  $\sim 2.2$  V, specific conductivity of few  $10^{-3} \Omega^{-1} \text{cm}^{-1}$ , and as high as 100% Coulombic reversibility. The main disadvantage of these electrolytes is their limited electrochemical anodic stability that limits its utilization in high-energy density cells. The limited anodic stability of these electrolytes was proved to be due to the relatively weak aluminum–carbon bond that electrochemically breaks via  $\beta$ -H-elimination.<sup>2,4</sup>

Hence, we theorized that substituting the aliphatic ligands for phenyl, which does not possess  $\beta$  hydrogen, will immunize the complex salts to this oxidation pathway. Indeed, cyclic

voltammograms (CV) with Pt working electrode, displayed electrochemical windows in excess of 3.3 V vs. Mg.<sup>5</sup> Additionally, these solutions possess specific conductivity of  $\sim 2 \times 10^{-3} \Omega^{-1} \text{cm}^{-1}$  at RT, and high Mg cycling efficiency. The widened electrochemical stability window attained with the all phenyl complex (APC)-type electrolytes is critical for future improvements of feasible rechargeable magnesium batteries, particularly with respect to energy density.

In previous papers, we reported on the structural analyses of the DCC family of electrolytes.<sup>1-4,6</sup> The current study follows a similar methodology for the complete identification of the whole range of species existing in the APC solutions.

In addition to the field of magnesium electrochemistry and rechargeable batteries, these families of organometallic molecules and their exact structures play central roles in high performance polymerization schemes as specific function catalysts.

## EXPERIMENTAL SECTION

All the chemical syntheses and electrochemical measurements were carried out under pure argon atmosphere (99.999%) in a M. Braun, Inc. glovebox (less than 1 ppm of water and oxygen).

**Chemicals and Syntheses.** All electrolyte solutions were synthesized according to the same procedure: First,  $\text{AlCl}_3$  (Aldrich, anhydrous, 99.999%) in THF (Aldrich, 99.9%, less than 20 ppm water) solution was

Received: December 5, 2010

Published: April 01, 2011

prepared in the desired concentration by very slow addition to the vigorously stirred solvent. Then, this solution was added dropwise to a predetermined quantity of 2 M Phenylmagnesiumchloride (PhMgCl) solution in THF (Aldrich). Both reactions are very exothermic. The resulting solution was stirred for additional 16 h or more (at room temperature).

The family of electrolytes containing phenyl ligands in various proportions is referred to in this paper as “APC”. Electrolyte concentrations were reported in terms of the aluminum-based species concentration. If not indicated otherwise, the  $\text{AlCl}_3$  to PhMgCl ratio is 1:2. Thus, a 0.25 M APC solution is synthesized by reacting equal quantities of 0.25 M  $\text{AlCl}_3$  and 0.5 M PhMgCl in THF. The standard electrolyte, to which others are compared, is 0.25 M APC, as it exhibits favorable electrochemical properties. In cases where solutions were prepared with  $\text{AlCl}_3$  and PhMgCl at ratios other than 1:2, they are denoted as APC  $m:n$  solutions ( $m$  and  $n$  are the relative amounts of  $\text{AlCl}_3$  and PhMgCl, respectively).

**Synthesis of  $\text{AlPh}_3 \cdot \text{THF}$  Reference Compound<sup>7</sup>.** A 2 M THF solution of phenylmagnesium chloride (22.5 mmol) was slowly added to a 1.2 M solution of  $\text{AlCl}_3$  (1.0 g, 7.5 mmol) in THF (6.25 mL) at 0 °C. The solution was then stirred for 14 h at RT, after which, the solvent was removed under reduced pressure. The solid residue (mainly  $\text{MgCl}_2$ ) was separated and removed by toluene extraction and centrifuging. The white powder left after toluene removal contained mainly  $\text{Ph}_3\text{Al} \cdot \text{THF}$  with less than 10% (molar)  $\text{MgCl}_2$ . NMR indicated a Ph:THF ratio of 3:1 (see Figure S1, Supporting Information [SI]).

Other syntheses followed well-documented procedures, and are similar to the one above.

**Elemental compositions (Al, Mg, Cl):** were determined by ICP and SM-4500-Cl<sup>-</sup> D (for Cl) at Aminolab Inc. (analytical laboratories) Israel. For these measurements, solution samples of 2 mL were withdrawn and reacted with 40 mL of doubly distilled water, to which few drops of concentrated nitric acid (Merck, 65%, extra pure) were added. Extra dry THF and other solvents were further dehydrated with activated 4A molecular sieves (Aldrich 4 Å, beads, 8–12 mesh). Trace water was monitored by Karl Fischer titration with Metrohm 652 KF coulometer.

**Spectral Studies.** Raman spectra were measured with a JY Horiba spectrometer using a He–Ne laser (632.817 nm) in screw-cap rectangular spectrozile quartz cuvettes. All experiments were performed at RT ( $25 \pm 4$  °C). We focused on the 100–1150  $\text{cm}^{-1}$  spectral region, which was found to be the most informative for the identification of the organometallic compounds.

NMR spectra were measured with a Bruker DMX-600 spectrometer.

**DFT Computations.** All aluminum core geometry optimizations were performed at the B3LYP/6-31+G\* level of theory.<sup>8–10</sup> Magnesium core geometry optimizations were done at the B3LYP/CEP-31+G\* level in the gas-phase and in solution. The solvent (THF,  $\epsilon = 7.58$ ) was taken into account via the IEFPCM model.<sup>11</sup> We failed to minimize the solvated  $\text{PhAlCl}_3^-$  molecule at the B3LYP/6-31+G\* due to a very flat potential energy surface; the optimization of this molecule was done at the B3LYP/6-31G\* with a single point calculation at B3LYP/6-31+G\*. Optimization at MP2/6-31+G\*\* and B3LYP/6-31+G\*\* levels gave nearly identical results.

Theoretical Raman spectra were calculated at the B3LYP/6-31+G\* level in the gas phase. A scaling factor of 0.965 was applied.<sup>12</sup> Insights regarding electron distributions were gained by natural bond analysis<sup>13</sup> (NBO), performed using B3LYP/6-31+G\*. All NBO and energy calculation were performed in solution using Gaussian 09 package.<sup>14</sup>

**Electrochemistry.** Electrochemical measurements were performed with an EG&G PAR 273 potentiostat controlled by “Corrware” software (Scribner, Inc.). Magnesium foils served both as the counter and reference electrodes in three-electrode cells. Flame-cleaned platinum wire working electrodes were used for studying the Mg deposition-dissolution processes and the anodic stability window of the solutions, which was determined at the deflection point in their potentiodynamic

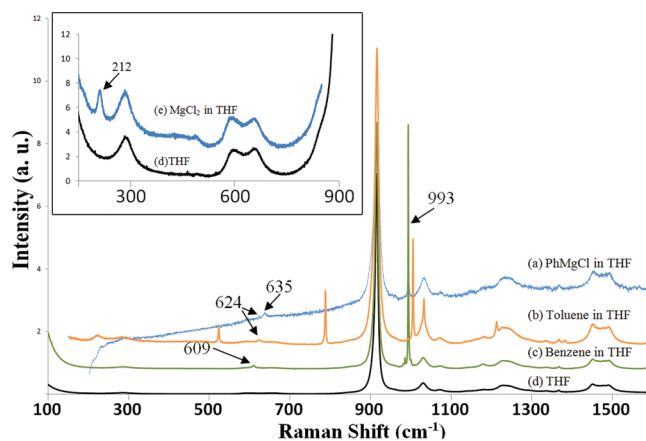


**Figure 1.** Raman spectra of (a) 0.5 M PhMgCl in THF in comparison with reference spectra, all in THF (top to bottom): (b) toluene, (c) benzene, and (d) THF. (Inset) (e)  $\text{MgCl}_2$  in THF in comparison to THF.

response, where the  $I$  vs  $E$  curves showed an appreciable increase in the positive currents. Preparative, potentiostatic [3.00 V vs Mg] electrolysis was carried out in a single compartment cell, passing 150 C ( $\sim 4$  h) (accounts to approximately 2 electrons per half the total amount of anions). Magnesium foil served as the counter and reference electrode [60  $\text{cm}^2$ ], and stainless steel net [24.5  $\text{cm}^2$ ] served as the WE. Measurements were performed at  $27$  °C  $\pm 3$ .

**Single-Crystal XRD.** Single-crystals ( $\sim 1$ –4 mm) were selected, washed with dry THF, and transferred (slightly wet) in a sealed glass vial under argon, to the X-ray facility. The crystals were coated with inert crystallography oil and were flash-frozen with  $\sim 100$  K nitrogen. The measurements were carried out using the Bruker “Kappa Apex II” system. Data collection was performed at cryo-temperatures under nitrogen atmosphere with Mo  $K\alpha$ , 0.07103 nm, radiation @  $\phi$  and  $\omega$  scans. Structure calculation and refinement were performed with the SHELXS-97 program.

## RESULTS AND DISCUSSION

Preliminary NMR and Raman spectroscopy studies with APC-type solutions revealed that this chemical system is by no means simple. Not only did the spectra exhibit numerous features, some very weak and wide, there were also no spectral reference library upon which the identification of the species could be based on. Thus, as for the aliphatic system,<sup>6</sup> in order to realize a complete identification of the species we had to establish a comprehensive reference spectra library containing the various possible compounds.

Only a few magnesium species exist in the complex solutions,<sup>6</sup> the most important of which are  $\text{MgCl}_2$ ,  $\text{MgCl}^+$ ,  $\text{Mg}_2\text{Cl}_3^+$ ,  $\text{Ph}_2\text{Mg}$  and  $\text{PhMgCl}$ , all coordinated by THF. Contrary to a recent publication,<sup>15</sup> we assume that in all the above cationic Mg species, the magnesium atom is hexacoordinated by a combination of  $\text{Cl}^-$  and THF ligands (for instance, see Figure 2). At relatively low concentrations in THF, it is reasonable to assume that these compounds exist predominantly as monomers.<sup>16</sup>

Figure 1 presents the Raman spectra for 0.5 M PhMgCl in THF, and for comparison, pure THF, toluene and benzene in THF.

As can be seen in Figure 1, the spectrum of THF over this region is characterized by six peaks: 289 (low and wide), 585 and 655 (very low and wide—seen for clarity in the inset) 914 (very high), 1031 (medium), and 1072  $\text{cm}^{-1}$  (low).<sup>17</sup> The spectrum of toluene in THF exhibits the same set of peaks related to the solvent, plus additional peaks, of which the most important one

**Table 1. Summary of the Most Characteristic Peak Positions in Raman Spectra for Some Reference Materials (M = Al or Mg)**

species	peak position, $\text{cm}^{-1}$			
	type of vibration M–Ph		type of vibration M–Cl	
Ph–Mg–Cl	635 ( $'E_{2g}'$ )	993 ( $'B_{1u}'$ )		
$\text{MgCl}_2$			212	
$\text{AlCl}_3 \cdot \text{THF}$			330	
$\text{AlCl}_4^- \cdot \text{THF}$			180 ( $T_2$ )	348 ( $A_1$ )
THF	289	585–655	1031	1072
phenyl group	624 ( $'E_{2g}'$ )	$\sim 1000$		

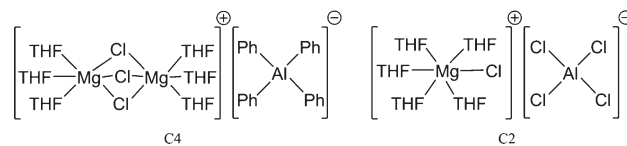
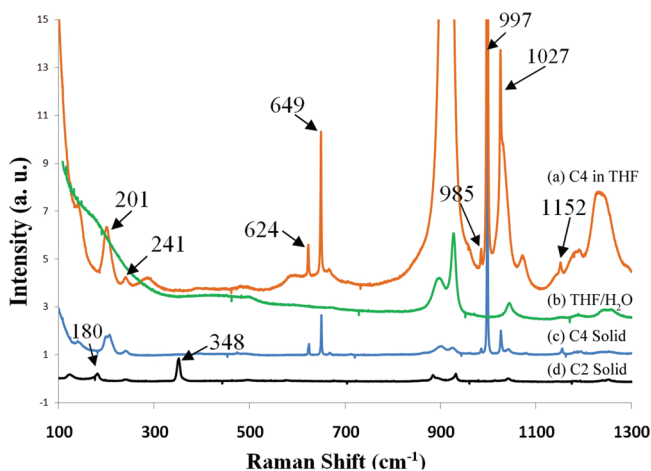
for this study is located at  $624 \text{ cm}^{-1}$  (denoted as  $'E_{2g}'$ , corresponding to the notation for benzene, pertaining to phenyl ring wagging, devoid of C–R stretching). As will be presented later, this peak appears whenever phenyl group is present in the system, regardless of its chemical environment, except for benzene. For benzene, as shown in Figure 1, this peak appears at  $609 \text{ cm}^{-1}$ . As will be seen later, the presence of a phenyl ligand invariably results in the appearance of peaks around  $1000 \text{ cm}^{-1}$  whose<sup>18</sup> specific location depends both on the core metal (magnesium or aluminum), and on the number of chlorine to phenyl ligands ratio. The spectrum of 0.5 M  $\text{PhMgCl}/\text{THF}$  displays three peaks, at 624 ( $'E_{2g}'$ ), 635 ( $'E_{2g}'$ ) (“represent the  $'E_{2g}'$  phenyl ring wagging, combined with C–R stretching”) and  $993 \text{ cm}^{-1}$  ( $'B_{1u}'$ ). The peak at  $635 \text{ cm}^{-1}$  is associated with a Ph–Mg vibration. The expected feature around  $1000 \text{ cm}^{-1}$  appears, in this case, as a single peak at  $993 \text{ cm}^{-1}$ . Unfortunately, the reference Raman spectrum for  $\text{Ph}_2\text{Mg}$  solution, synthesized according to standard procedure<sup>19</sup> showed only the THF peak at  $914 \text{ cm}^{-1}$  due to strong fluorescence. In a previous Raman study<sup>6</sup> we showed that  $\text{MgCl}_2$  in THF (inset) displays a single characteristic peak, at  $212 \text{ cm}^{-1}$ . For further identification of the Raman bands we were assisted by the results from the DFT calculations. Figure S2 (SI) exemplifies the close correlation between the DFT calculated and the experimental spectra.

In the course of establishing a reliable reference library of spectra, we also measured the spectra of various aluminum compounds containing only chlorine ligands (see Figure S3, SI).

Table 1 summarizes the relevant peaks for the above reference materials.

Previous studies have shown that the transmetalation reactions between organo–halo aluminum and magnesium compounds can be understood in terms of Lewis acid–Lewis base reactions.<sup>1–3</sup> The reactions are frequently very exothermic and result in new species, neutral and/or ionic, depending on the reactants concentration, ratio, reaction temperature, and the solvent used. In these reactions, the aluminum species are acidic, and the magnesium ones are bases. Three important characteristics were discovered regarding these reactions:

1. Aluminum is preferentially coordinated by organic ligands, while the magnesium is preferentially coordinated by chlorine and THF.
2. The final equilibrium species in the solution, whether ionic or neutral, depend on the relative acidity (basicity) of the products.
3. The equilibrium aluminum species are a mixture of various combinations of compounds, characterized by Cl/R ratios.<sup>1–3,5</sup>

**Figure 2. Structures of C4 and C2 solids (obtained from single-crystal XRD) precipitated from THF solutions of 0.4 M  $\text{AlCl}_3$  + 0.8 M  $\text{PhMgCl}$ , and of 0.25 M  $\text{AlCl}_3$  + 0.125 M  $\text{PhMgCl}$ , respectively.****Figure 3. Raman spectra of (a) redissolved C4 in THF (saturated), (b)  $\sim 1 \text{ M}$  THF in water, (c) solid C4 precipitated from solution composed of 0.4 M  $\text{AlCl}_3$  + 0.8 M  $\text{PhMgCl}$ , and (d) solid C2 precipitated from solution composed of 0.25 M  $\text{AlCl}_3$  + 0.125 M  $\text{PhMgCl}$ .**

When analyzing the electrochemical properties of such a complex solutions, the exact equilibrium species present in the solution are of paramount importance. Clear correlation was established between the chemical and the electrochemical characteristics of the solution, and its constituents for the DCC case.<sup>1–3,5</sup> Of the different solution-species, the one dominating the anodic stability limit is the most oxidation-vulnerable moiety.

When we first started exploring the solution structure of the phenyl ligand-containing complexes, we hypothesized that the same principles found previously for DCC solutions would also govern the reactions and the equilibrium products of this family of materials.<sup>5</sup> Indeed, when  $\text{PhMgCl}$  solution reacts with  $\text{AlCl}_3$  solution, a very exothermic reaction ensues, yielding a solution with high ionic conductivity, which testifies that new materials are being generated.<sup>5</sup>

As demonstrated below, for the APC solutions, the systems indeed undergo a complete trans-metalation of the organic ligands from magnesium to aluminum. However, in this case we obtain a unique mixture of organo–aluminum and chloro–aluminum species, of seemingly very different Lewis acidities, coexisting in equilibrium. This peculiar phenomenon is discussed further in the paper. The rich and complex mixture of anionic and molecular species, and occasionally precipitates, formed in APC solutions makes the analysis of even the simplest solutions extremely challenging.

For instance, transparent, colorless crystals precipitated from any solution made with 2:1 Al:Mg ratio, and in solutions with 1:2 Al:Mg, at 0.3 M or above, when synthesized at RT. Such crystals, C2 and C4, respectively, analyzed by single-crystal X-ray diffraction (SCXRD) and solid-state NMR. Figure 2 displays the results of the SCXRD.<sup>27</sup>  $^{27}\text{Al}$  SSNMR of C4 fully supported the SCXRD results (see Figure S5, SI).

Table 2. Calculated Raman Peak Positions for Organo–Halo Aluminum Anions and Molecules in THF

anion	peak position, $\text{cm}^{-1}$			molecule	peak position, $\text{cm}^{-1}$		
$\text{Ph}_4\text{Al}^-$	186	614 ( $E_{2g}$ )	638 ( $E_{2g}$ )				
$\text{Ph}_3\text{AlCl}^-$	193	614 ( $E_{2g}$ )	644 ( $E_{2g}$ )	$\text{Ph}_3\text{Al}\cdot\text{THF}^-$	196	614 ( $E_{2g}$ )	646 ( $E_{2g}$ )
$\text{Ph}_2\text{AlCl}_2^-$	252	614 ( $E_{2g}$ )	652 ( $E_{2g}$ )	$\text{Ph}_2\text{AlCl}\cdot\text{THF}$	272	614 ( $E_{2g}$ )	657 ( $E_{2g}$ )
$\text{PhAlCl}_3^-$	276	614 ( $E_{2g}$ )	662 ( $E_{2g}$ )	$\text{PhAlCl}_2\cdot\text{THF}$	275	613 ( $E_{2g}$ )	672 ( $E_{2g}$ )
$\text{AlCl}_4^-$	107 (E)	167 (T <sub>2</sub> )	326 (A <sub>1</sub> )				

The Raman spectra of these crystals, containing the unambiguously identified  $\text{Mg}_2\text{Cl}_3^+$ ,  $\text{Ph}_4\text{Al}^-$ , and  $\text{AlCl}_4^-$  species (coordinated by THF), were also used for the Raman spectra library. Figure 3 displays the Raman spectra of C4 (solid), C2 (solid), and redissolved C4 saturated solution in THF.

C4 (c) and C2 (d) spectra are very unique, as they exhibit unambiguously identified components, one for each metal core, with the addition of crystal-bound THF. The crystal-bound THF spectral characteristics, as expected, are somewhat different from those of the free THF. In these spectra the main THF peak at  $914\text{ cm}^{-1}$  splits into two narrow peaks.<sup>17</sup> In order to confirm that these peaks indeed belong to THF, we dissolved  $\sim 1\text{ M}$  THF in water [see Figure 3b]. In this state the THF molecules are solvated by water, and thus, presumably, lack THF–THF interactions. This assisted in identifying and excluding all the crystal-bound THF peaks appearing in the C4 and C2 solids spectra. The C2 crystal exhibits only four peaks, neglecting the THF ones: three at 115(E), 180(T<sub>2</sub>), and 348(A<sub>1</sub>)  $\text{cm}^{-1}$ , attributed to  $\text{AlCl}_4^-$ . The very weak feature at  $241\text{ cm}^{-1}$ , pertaining<sup>6</sup> to  $\text{Mg}_2\text{Cl}_3^+$ , is attributed to a minor residue. As did Sobota et al.<sup>17</sup> who also investigated similar complexes, we did not detect any features attributable to  $\text{MgCl}^+$ . Due to the low solubility of C2 in THF, no Raman spectrum of its solution could be obtained.

The C4 (c) spectrum displays clearly the expected  $\text{Mg}_2\text{Cl}_3^+$  peak as a strong feature at  $241\text{ cm}^{-1}$ . The other peaks, at 201, 624( $E_{2g}$ ), 649( $E_{2g}$ ), 985, 997, and  $1152\text{ cm}^{-1}$  are all attributed to the symmetrical tetraphenyl aluminate ion. The peak at  $624\text{ cm}^{-1}$  invariably appears whenever a phenyl group is present in the system.

Interestingly, as can be seen in spectra (a) and (c) of Figure 3, there is no difference in the peak positions for C4 as solid crystal or as THF solution. This later allowed with great certainty the identification of the existence of both  $\text{Mg}_2\text{Cl}_3^+$  and  $\text{Ph}_4\text{Al}^-$  in solutions. Spectrum (a) is characterized by five unique peaks, at 201, 649( $E_{2g}$ ), 985, 997, and  $1152\text{ cm}^{-1}$ . As gathered from the NMR, elemental analysis, and the Raman spectra, the peaks in the  $1000\text{ cm}^{-1}$  region pertain solely to phenyl ligands around the aluminum core. The exact peak positions change very little with the nature of the aluminum-core molecule or ion, regardless of the Ph:Cl ratio. The 201 and  $649\text{ cm}^{-1}$  peaks, on the other hand, are exclusive to  $\text{Ph}_4\text{Al}^-$ , and exist both for the solid C4 crystal, and its solution, though with some peak-shape difference for the  $201\text{ cm}^{-1}$  peak.

We calculated the Raman spectra for the five possible  $\text{Ph}_y\text{AlCl}_{4-y}^-$  ions ( $y = 0-4$ ), and their neutral forms, focusing only on the most significant (intense) peaks. Each molecule has a single strong peak in the  $250\text{ cm}^{-1}$  region and two strong peaks in the  $650\text{ cm}^{-1}$  region. Table 2 summarizes the relevant calculated peaks for these materials:

Not only these bands are the most intense in the specified region, but also each column represents the same vibrational mode, as judged from visualization of the normal vibrational modes. For instance, the  $614\text{ cm}^{-1}$  band pertains to phenyl ring

wagging ( $E_{2g}$ ), devoid of C–Al stretching, and the peaks in the  $638-662\text{ cm}^{-1}$  region relate, in all cases, to the ring stretching ( $E_{2g}$ ) mode, combined with C–Al stretching. The appearance of distinct and unique bands for each of the different ions allows the identification of the aluminum core species in the solutions, based solely on Raman spectroscopy.

Several interesting observations and trends may be deduced from the calculated data and their relation to the measured values (Table 2). First, as can be seen from the listed values, the calculated spectra predict a clear trend for the first and third row peak positions versus Ph:Cl ratio. The higher this ratio, the higher the peak position in  $\text{cm}^{-1}$ , although the computed vibrations are consistently lower than the experimental ones. Additionally, the peaks associated with the middle column are practically constant, regardless of the Ph:Cl ratio, both for the measured and the calculated spectra. This result is expected as the  $E_{2g}$  vibration, at  $624\text{ cm}^{-1}$  involved only the benzene-ring bonds.

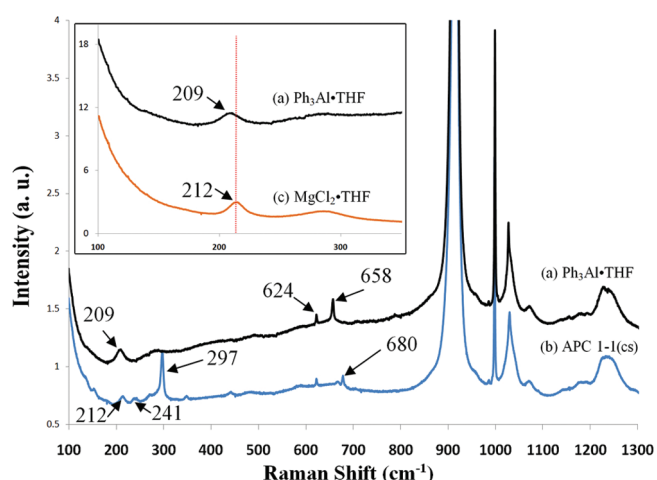
Previous multinuclear NMR analysis<sup>3</sup> of a homologue series of compounds containing aliphatic ligands showed clearly that the  $^{27}\text{Al}$  NMR spectra for the anions  $\text{R}_y\text{AlCl}_{4-y}^-$  and the molecules  $\text{R}_y\text{AlCl}_{3-y}\cdot\text{THF}$  ( $y = 1-4$ ;  $y' = 1-3$ ) are identical whenever  $y = y'$ ; e.g.  $\text{R}_2\text{AlCl}_2^-$  exhibits the same spectrum as  $\text{R}_2\text{AlCl}\cdot\text{THF}$ . Hence, from  $^{27}\text{Al}$  NMR analysis point of view, the  $\text{Cl}^-$  ligand has the same influence on the chemical shift as THF. Interestingly, we observed a similar trend in the Raman spectra for the Al core anions and the neutral molecules in the current study. For instance, the most important features of the calculated and experimental Raman spectra for  $\text{Ph}_3\text{AlCl}^-$  are very similar to those for  $\text{Ph}_3\text{Al}\cdot\text{THF}$ . The calculated Raman spectra show the same trend for all the vibrations, except for the lowest vibration for  $\text{Ph}_2\text{AlCl}_2^-$  and  $\text{Ph}_2\text{AlCl}\cdot\text{THF}$  ( $252$  and  $272\text{ cm}^{-1}$ , respectively). However, careful  $^{13}\text{C}$  NMR analysis of the spectra of a wide range of anionic and neutral species indicated small but significant and consistent differences that make a distinction between these species. Based on these results (to be published soon) we conclude that no detectable levels of aluminum-based neutral compounds exist in the above solutions.

It is worth mentioning that the peak at  $201\text{ cm}^{-1}$  in the C4 spectrum is very close to the  $212\text{ cm}^{-1}$  peak of  $\text{MgCl}_2$ , and to one for the calculated  $\text{Ph}_3\text{AlCl}^-$  peak. This, in some cases, hampers the unambiguous identification of all the components in some of the more species-rich solutions.

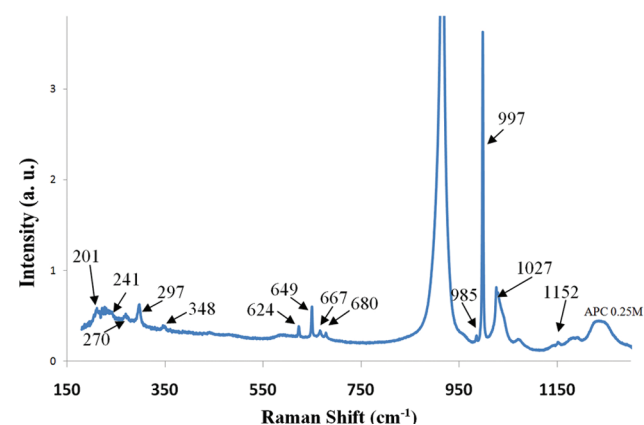
Two important reference solutions provided important spectral information:  $\text{Ph}_3\text{Al}\cdot\text{THF}$  in THF and an APC solution containing  $\text{PhAlCl}_3^-$  as the major anion. The later solution, APC 1:1 (cs), was synthesized by reacting equimolar quantities of  $\text{PhMgCl}$  with  $\text{AlCl}_3$  in THF at  $0^\circ\text{C}$ . NMR analysis indicated that this solution contains  $\text{PhAlCl}_3^-$  as the major anionic product plus low concentration of  $\text{Ph}_2\text{AlCl}_2^-$  (see Figure S6, SI).

Figure 4 displays the Raman spectra of  $\text{Ph}_3\text{Al}\cdot\text{THF}/\text{THF}$  and APC 1:1 (cs) solutions.

As can be seen in Figure 4, both  $\text{Ph}_3\text{Al}\cdot\text{THF}$  and APC 1:1 (cs) solutions exhibit the expected peaks at 624, 985, 997, and



**Figure 4.** Raman spectra of (a)  $\text{Ph}_3\text{Al}$  in THF (b) solution made by reacting 0.25 M  $\text{AlCl}_3$  + 0.25 M  $\text{PhMgCl}$  (APC 1:1 (cs)) in THF at 0 °C. (Inset) Comparison between (a)  $\text{Ph}_3\text{Al}$  in THF and (c)  $\text{MgCl}_2$  in THF. [(cs) = cold temperature synthesis].



**Figure 5.** Raman spectrum of a standard 0.25 M APC solution (0.25 M  $\text{AlCl}_3$  + 0.5 M  $\text{PhMgCl}$  in THF).

$1152\text{ cm}^{-1}$ , the common features for phenyl containing aluminum species. The  $\text{Ph}_3\text{Al}\cdot\text{THF}$  spectrum contains additional peaks, at 209 and  $658\text{ cm}^{-1}$ , predicted also from the calculated spectra (see Table 2, data for  $\text{Ph}_3\text{AlCl}^-$ ). Despite the proximity of  $\text{MgCl}_2$  and  $\text{Ph}_3\text{Al}$  peaks, the two features are exclusive, and can be used to identify the existence of each of them with certainty. This is exemplified in the inset in Figure 4. The spectrum of this solution shows a prominent peak at  $680\text{ cm}^{-1}$  as the strongest feature in the region of  $650\text{ cm}^{-1}$ . It also possesses a peak at  $297\text{ cm}^{-1}$ , as the strongest band in this spectral region. The existence of the two species,  $\text{Ph}_2\text{AlCl}_2^-$  and  $\text{PhAlCl}_3^-$ , at approximately 1:5 ratio can clearly be identified from the Raman spectrum, with solid support from the calculated data and the NMR spectrum (see Figure S6, SI). The spectrum also shows the expected  $\text{MgCl}_2$  and  $\text{Mg}_2\text{Cl}_3^+$  peaks at 212 and  $241\text{ cm}^{-1}$ , respectively.

After identifying the main species that might exist in the complex electrolytes and establishing a reference spectra library, we elaborated on the identification of the equilibrium species in the “standard” APC solution (i.e.,  $\text{AlCl}_3$  and  $\text{PhMgCl}$  at 1:2 ratio).

Figure 5 displays the Raman spectrum of a standard 0.25 M APC solution, at room temperature.

**Table 3. Summary of Peak Positions for the Measured Raman Spectra of Organo–Halo Aluminum and Magnesium Species in THF**

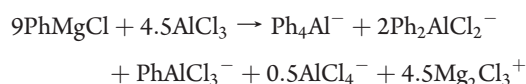
species	peak position, $\text{cm}^{-1}$
$\text{PhMgCl}\cdot n\text{THF}$	$624^a$ 635 993
$\text{PhAlCl}_3^-/\text{PhAlCl}_2\cdot\text{THF}$	297 624 680 985 997 1027 1152
$\text{Ph}_2\text{AlCl}_2^-/\text{Ph}_2\text{AlCl}\cdot\text{THF}$	270 624 667 985 997 1027 1152
$\text{Ph}_3\text{AlCl}^-/\text{Ph}_3\text{Al}\cdot\text{THF}$	209 624 658 985 997 1027 1152
$\text{Ph}_4\text{Al}^-$	201 624 649 985 997 1027 1152
$\text{MgCl}_2\cdot 4\text{THF}$	212
$\text{Mg}_2\text{Cl}_3^+\cdot 6\text{THF}$	241
$\text{MgCl}^+\cdot 5\text{THF}$	unknown
$\text{AlCl}_3\cdot\text{THF}$	330 860
$\text{AlCl}_4^-$	$180(\text{T}_2)$ $348(\text{A}_1)$

<sup>a</sup>The  $600\text{ cm}^{-1}$  region vibrations pertain to  $\text{E}_{2g}$ .

This spectrum reflects the coexistence of a wide variety of aluminum species, with  $\text{Mg}_2\text{Cl}_3^+$  as the major magnesium species. All the peaks discernible in Figure 5, apart from the two at 270 and  $667\text{ cm}^{-1}$ , have already been identified and presented in Figures 2–4 and S2–S3 (SI). On the basis of the various possibilities for Al-containing solution species and the NMR data, we hypothesized that these two peaks pertain to  $\text{Ph}_2\text{AlCl}_2^-$ . Moreover, this pair of peaks and their approximate positions were predicted by the theoretical calculations. It is important to recognize, as can be inferred from the multitude of features in the  $650\text{ cm}^{-1}$  and the  $250\text{ cm}^{-1}$  regions, that this solution contains almost all possible organo–halo aluminum species. Furthermore, the spectrum contains no features attributed to raw materials, proving that the trans-metalation reaction goes to completion. NMR spectroscopy supports all of these conclusions, as is further reported.

Table 3 summarizes the dominant experimental Raman vibrational bands for the most important magnesium and aluminum core species.

From Table 3 and Figure 5 it is deduced that the equilibrium species present in the standard APC solution are  $\text{Ph}_4\text{Al}^-$ ,  $\text{Ph}_2\text{AlCl}_2^-$ ,  $\text{PhAlCl}_3^-$ ,  $\text{AlCl}_4^-$  and  $\text{Mg}_2\text{Cl}_3^+$ . This list takes into account only anionic aluminum species, as inferred from the high ionic conductivity, of  $1.8 \times 10^{-3}\ \Omega^{-1}\text{ cm}^{-1}$ , and the  $^{13}\text{C}$  NMR analyses. On the basis of these data, the following reaction formula (APC electrolyte formation scheme and solution equilibrium species) is suggested for the formation of the standard APC solution:



As noted at the beginning of this paper, the explicit electrochemical characteristics of the complex solutions is dominated by the various equilibrium species existing in the solution. This, in turn, is very sensitive to a variety of factors, such as the total concentration, solvent, components ratio (R:Mg:Al:Cl), and even the preparation procedure. In Figures S7 and S8 (SI) the influence of the synthesis temperature and the total complex concentration is analyzed, as well as LiCl addition.

The results presented in Figures S7 and S8 (SI) prove that LiCl acts as a  $\text{Cl}^-$  donor in the APC system. Nonetheless, one striking difference between the DCC and the APC electrolytes solutions is reflected in these results. In contrast to the case of DCC solutions, APC solutions form rather puzzling solution equilibria. As studied

**Table 4. Summary of the HOMO and LUMO Energy Levels and Their Energy Difference in eV for the Halo–Organo Aluminum and Magnesium Species in THF**

molecule	energy level (eV)		$\Delta$
	HOMO	LUMO	
$\text{Ph}_4\text{Al}^-$	-5.33	0.64	5.97
$\text{Ph}_3\text{AlCl}^-$	-5.76	0.38	6.15
$\text{Ph}_2\text{AlCl}_2^-$	-5.98	0.34	6.32
$\text{PhAlCl}_3^-$	-6.20	0.23	6.43
$\text{Ph}_3\text{Al} \cdot \text{THF}$	-6.55	-0.62	5.93
$\text{Ph}_2\text{AlCl} \cdot \text{THF}$	-6.71	-0.71	6.00
$\text{PhAlCl}_2 \cdot \text{THF}$	-6.99	-0.77	6.22
$\text{MgCl}^+ \cdot \text{THF}_5$	-7.46	-0.79	6.67
$\text{Mg}_2\text{Cl}_3^+ \cdot \text{THF}_6$	-7.51	-0.69	6.82
$\text{AlCl}_4^-$	-7.53	1.01	8.54

from the spectrum in Figure S8 (SI), the equilibrium species exhibit coexistence of a wide variety of aluminum compounds, among which are  $\text{AlCl}_4^-$  and  $\text{Ph}_4\text{Al}^-$ . This is a very unusual situation, as these two compounds (as well as all the other aluminum core species in this solution) are expected to exhibit two extremes of Lewis acidity. This is in striking contrast to the DCC electrolytes family, which usually contain either a single aluminum-based species in the solution or the smallest possible variety of species, forming a uniform mixture of  $\text{Cl}^-$  (or THF) and organic ligands around the aluminum core. The origin of this phenomenon is not yet understood.

The comprehensive spectral analysis presented above led to the identification of the various species coexisting in equilibrium in APC-type solutions. One of the important characteristics of the APC electrolytic solution, in contrast to DCC, is its apparent wide electrochemical stability window. The anodic stability limit for any electrochemical system is dominated by its most oxidation susceptible component. For the APC family of solutions, it is expected that the most oxidation vulnerable component would be a molecule or an ion containing the weakest metal–carbon bond. Since none of these solutions include organo–magnesium compounds, the weakest link is predicted to contain an aluminum–carbon bond. It was shown in studies with the DCC family of electrolytes that, as a rule of thumb, the greater the Cl:Al ratio, the higher its electrochemical oxidation potential. In other words, the more inorganic character the aluminum species possesses, the greater its oxidation stability.

The relative stability toward oxidation may be evaluated, experimentally, using electrochemistry. In the simplest case, cyclic voltammetry (CV) with inert working electrode can be utilized for this purpose. Keeping all the experimental setup and conditions constant, the anodic stability window can be determined as the deflection point in the positive scan where the current increases appreciably. It is also possible to estimate the relative sensitivity toward oxidation from the calculated molecular orbital HOMO energies, as the oxidation reaction involves removal of an electron from the compound's HOMO level.<sup>20</sup>

Table 4 summarizes the calculated HOMO and LUMO energy levels for a variety of halo–organic aluminum and magnesium species, in THF, and the pure solvent. The values listed were calculated for the structure-optimized species, as explained in the Experimental Section, including the THF solvent influence. Considering the organometallic species only, a clear trend is obtained from this table. As predicted, the greater

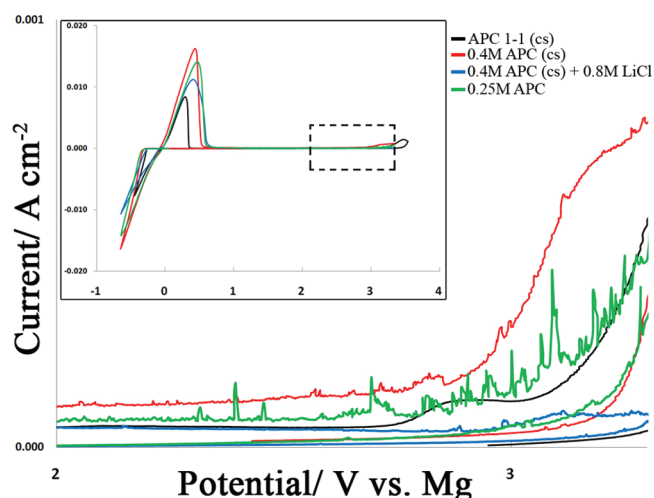


**Figure 6.** Steady-state cyclic voltammograms of four APC electrolyte solutions, measured with Pt wire working electrodes, Mg strips as counter, and reference electrodes at 25 mV/s.

the Cl:Al ratio, the lower its HOMO energy level, and therefore the greater its expected stability toward oxidation.

In relation to the relevant organo–halo species only, these results predict  $\text{Ph}_4\text{Al}^-$  to be the most oxidation vulnerable species, while  $\text{AlCl}_4^-$  to show the greatest stability. Thus, electrochemically, we can conclude that any noticeable concentration of  $\text{Ph}_4\text{Al}^-$  will have detrimental influence on the solution anodic stability limit. The same argument applies to all other APC-type solutions, in such a way that the presence of the most oxidation-prone species will govern the anodic stability window for the whole system. As such, the weakest link in the chain is the species containing the highest Ph:Cl ratio. The picture described in this section ignores the anodic stability of pure THF, and THF in the presence of the solution species. Based on the literature-reported oxidation stability window of  $\sim 4.5$  V vs Li for THF in a variety of systems<sup>21</sup> and the rule of thumb that puts the magnesium deposition–dissolution at roughly 1 V above lithium, the anodic stability limit for THF in the magnesium scale is estimated to lie around 3.5 V, far above the anodic stability windows measured for most APC-type solutions. Support for this hypothesis was found in a preparative electrolysis experiment that we have carried out with an APC solution, in which the main product was found to be benzene, presumably due to the electrochemical breakdown of phenyl–aluminum bonds. No THF oxidation products were detected (see Figure S9, SI).

In order to investigate whether the theoretical calculations predict the experimental results adequately, we performed cyclic voltammetry with a variety of APC electrolyte solutions.

Figure 6 displays the anodic side of CVs for several APC solutions with Pt working electrodes. The inset in this figure shows the full CVs (including the reversible Mg deposition domain at the left-hand side of the voltammogram) with the potential domain of interest marked.

The four APC solutions' CVs presented in Figure 6 contain, according to the spectral analysis described above, the following oxidizable species: APC 1:1 (cs) contains  $\text{PhAlCl}_3^-$  and  $\text{Ph}_2\text{AlCl}_2^-$ ; 0.4 M APC (cs) contains all the various aluminum core species, including  $\text{Ph}_4\text{Al}^-$ , and so does the 0.25 M APC solution (see Figure S7, SI); 0.4 M APC (cs) solution with the addition of 0.8 M LiCl contains chiefly  $\text{Ph}_4\text{Al}^-$  and  $\text{AlCl}_4^-$ . Thus, considering the arguments presented above, we expected that all other CV's will show

lower anodic stability window than that for APC 1:1 (cs), which contains no  $\text{Ph}_4\text{Al}^-$ . Unexpectedly, Figure 6 reveals, among other things, that this is not the case. The CVs show that regardless of the identity of the solution species, discernible oxidation currents commence at around 2.7–2.9 V. For instance, APC 1:1 (cs) solution, which was expected to show the highest anodic stability, starts to oxidize at as low as  $\sim 2.7$  V, while 0.4 M APC (cs) containing 0.8 M LiCl, which was predicted to possess the lowest anodic stability, does not show appreciable oxidation currents at up to 3.1 V. It is important to note that this CV does exhibit a deflection point in the positive currents at  $\sim 2.9$  V. However, in contrast to the other cases, after the slight increase in the currents, it stabilizes and even shows decrease in the oxidation currents. In the usual cases, following the deflection point, the currents continue to increase steadily, rapidly reaching substantial values (as the potentials are higher).

Whatever the reason for the observed exceptional anodic stability of the APC electrolytes is, recent important measurements revealed unequivocally that these electrolyte solutions are indeed very promising candidates for practical high energy density, high voltage, magnesium batteries. In these experiments we reversibly intercalated/deintercalated lithium ions into two cathode materials, namely  $\text{V}_2\text{O}_5$  and  $\text{LiFe}_{0.2}\text{Mn}_{0.8}\text{PO}_4$  in APC solutions containing 0.5 M LiCl within the potential window of  $-0.8$  to 3 V vs Mg (a detailed description of these studies is beyond the scope of this paper). The reversible insertion of Li ions into these systems testifies that the APC solution is anodically stable at least up to 2.8 V vs Mg.

In almost all CVs carried out with APC-type solutions with Pt as WE, as seen very clearly in Figure 6 for 0.25 APC solution, the anodic side of the CV is characterized by random, positive current spikes. We hypothesize that this phenomenon relates to kind of quasi-passivation of the Pt electrode by solution species. This behavior is unique to APC type solutions, and was not observed for the DCC-type solutions. Hence, we theorize that the aromatic phenyl groups are responsible for this unique behavior. We suspect that specific adsorption of the aromatic Al–Ph-containing molecules onto the platinum surface plays an important role in this phenomenon, leading to the unexpected anodic stability of these solutions. The spiky CVs observed for many APC solutions in the anodic domain are hypothesized to be a manifestation of a break-and-repair-like mechanism. Such mechanism may explain the unpredictably high anodic stability for 0.4 M APC (cs) containing 0.8 M LiCl that contains the largest  $\text{Ph}_4\text{Al}^-$  concentration. This also may explain the insensitivity of the anodic stability window measured for many APC-like solutions with platinum. Support for this assumption can be obtained from a closer examination of the CVs in Figure 6, particularly in the 2.8–2.9 V region. As can be seen, even the CV for 0.4 M APC (cs) solution containing 0.8 M LiCl, which does not attain substantial oxidation currents at up to 3.0 V, clearly shows a positive deflection point in the current. However, soon after this rise in current, the current density evens out, and even decreases a little, suggesting that the electrochemical activity is inhibited. The exploration of this phenomenon deserves comprehensive electrochemical and surface analysis studies.

In order to shed some light on the mechanism through which the organo–halo aluminum species undergo electrooxidation, we visualized the natural bond orbitals (NBO) for selected phenylaluminum chloride molecules and anions. This is exemplified below for  $\text{Ph}_3\text{AlCl}^-$ . The picture obtained indicates that the highest lying HOMO orbital is located at the aromatic  $\pi$ -systems of the phenyl ligands, as seen in Figure 7.

These observations lead us to suggest that the first stage in the electrooxidation process commences by electron abstraction

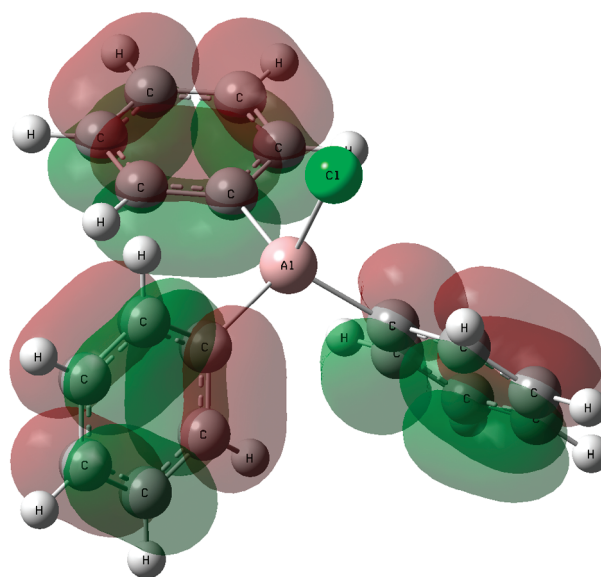


Figure 7. Visualization of the HOMO NBO for  $\text{Ph}_3\text{AlCl}^-$  in THF.

from the aromatic system of the phenyl ligands, probably yielding a phenyl radical. According to the electrolysis results reported above, indeed the Al–C bond between the phenyl ligand and the aluminum core breaks down. At this stage we have no further information as to the entire set of final reaction products. We have no data regarding the Al-based compounds, nor do we know from which species the phenyl radical captures hydrogen to yield the main product, benzene, although it is very probable that it takes it from THF.

The NBO analysis for the entire range of the aluminum-based species in this study reveals an interesting phenomenon. For all the chlorophenyl aluminum species, the DFT calculations yield aromatic phenyl rings in the expected alternating order of  $\sigma$ - and  $\pi$ -bonds. However, for  $\text{PhAlCl}_3^-$ , which contains the largest number of electron-withdrawing chlorine ligands, the NBO calculated molecule shows clear breakdown in the aromaticity of the phenyl ring. As seen in Figure 8, the NBO's HOMO level is suggestive of a quinone-like structure, with two double and four single bonds.

This phenomenon, which is also obtained with higher computation levels, e.g. B3LYP/6-31+G(d,p), MP2/6-31(d,p), can be studied using the NBO occupancy analysis (see Table. S10). It can be attributed to the strong electron-withdrawing capacity of the triply chlorinated aluminum core, imparting excess positive charge on the organic ligand. The same phenomenon is found also for  $\text{PhAlCl}_2 \cdot \text{THF}$ . Additional support for this phenomenon is presented in Figure S11, SI.

Similar quinoid structures were reported for substituted benzene rings, and for quinone-methide.<sup>22–24</sup> Analysis of the NBO models shows that despite the quinoid character of the ring in this case, all the C–C and C–H bond lengths remain practically identical, as in the aromatic systems.<sup>25,26</sup> However, analysis of the C–C–C bond angles within the rings of  $\text{PhAlCl}_3^-$ , as presented in Table 5, does show that unusual distortion occurs in the ipso position, relative to the other anions. Only slight differences are calculated for the C–C–C angles in the other positions, namely ortho, meta, and para.

Unfortunately, experimental validation of this phenomenon could not be obtained from the Raman and NMR measurements. As reported above, the changes in the spectral data versus the Cl: Ph ratio show only gradual changes.

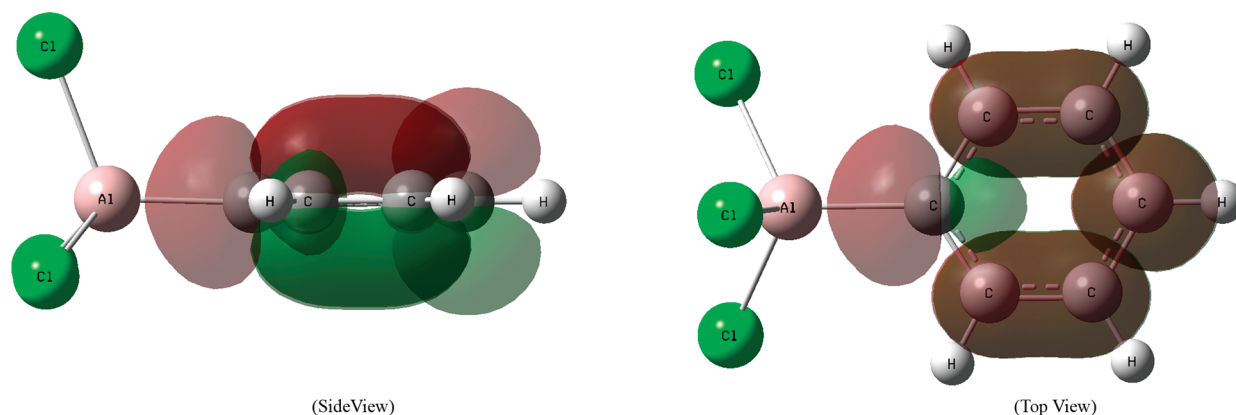


Figure 8. Visualization of the HOMO NBO for  $\text{PhAlCl}_3^-$  in THF.

Table 5. Summary of C–C–C Bond Angles (deg) for the Phenyl Rings in  $\text{Ph}_y\text{AlCl}_{4-y}^-$  Ions ( $i$  = ipso,  $o$  = ortho,  $m$  = meta,  $p$  = para carbon)

anion	$\theta_i$	$\theta_o$	$\theta_m$	$\theta_p$
$\text{Ph}_4\text{Al}^-$	115.37	122.78	119.95	119.145
$\text{Ph}_3\text{AlCl}^-$	115.77	122.51	119.96	119.27
$\text{Ph}_2\text{AlCl}_2^-$	116.23	122.22	119.96	119.39
$\text{PhAlCl}_3^-$	116.53	122.03	120	119.4

Additional interesting information is revealed from the DFT-calculated structures pertaining to the ligand–aluminum bonds. In all cases the R–Al bond is established through a lone-pair on the ipso carbon, indicating polar–covalent/coordination bonds (see Figure S12, SI). The same type of bonding is also found for the Cl–Aluminum bonds. Interestingly, the bond lengths for all the ligands show a clear trend: the higher the Cl:Ph ratio, the shorter the Al–ligand bond length. This constitutes an additional point of view for the expected trend in bonds strengths, as found from the HOMO energy levels.

## CONCLUSIONS

We have identified the major equilibrium species constituting the electrolyte solutions formed by reacting  $\text{PhMgCl}$  and  $\text{AlCl}_3$  in THF. Raman spectroscopy, together with DFT calculations, NMR, and single-crystal XRD provided most of the evidence necessary for the elucidation of this complicated system. Some ambiguous and less clear issues remain, such as the existence of the elusive  $\text{MgCl}^+$  ion, which has only been identified in SCXRD, and the close spectral similarity between the anionic and neutral aluminum species. The various solution species in the APC family depend to a large extent, apart from the raw materials proportions, on the synthesis temperature. The oxidation stability trend among the computed aluminum-based compounds does not follow the experimental stability window. We assume that the anodic electrochemical behavior of these species is governed by an inhibiting mechanism, such as specific adsorption, that leads to quasi-passivation.

On the basis of this work, it appears that adequate selection of the raw materials, their stoichiometric ratios, and the synthesis conditions can yield solutions for rechargeable magnesium batteries with operating voltages in excess of 2.5 V (vs Mg). This presents an extension of more than 1 V compared to the first generation of the rechargeable Mg battery system presented a

decade ago. A further followup challenge is research and development of Mg insertion cathodes with redox potentials as high as 2.5 V in the Mg scale.

## ASSOCIATED CONTENT

**S Supporting Information.** Supplementary figures and complete ref 14. This material is available free of charge via the Internet at <http://pubs.acs.org>.

## AUTHOR INFORMATION

### Corresponding Author

[aurbach@mail.biu.ac.il](mailto:aurbach@mail.biu.ac.il)

## REFERENCES

- (1) Aurbach, D.; Lu, Z.; Schechter, A.; Gofer, Y.; Gizbar, H.; Turgeman, R.; Cohen, Y.; Moshkovich, M.; Levi, E. *Nature* **2000**, *407*, 724.
- (2) Aurbach, D.; Gizbar, H.; Schechter, A.; Chusid, O.; Gottlieb, H. E.; Gofer, Y.; Goldberg, I. *J. Electrochem. Soc.* **2002**, *149*, A115.
- (3) Gizbar, H.; Vestfrid, Y.; Chusid, O.; Gofer, Y.; Gottlieb, H. E.; Marks, V.; Aurbach, D. *Organometallics* **2004**, *23*, 3826.
- (4) Gofer, Y.; Chusid, O.; Gizbar, H.; Vestfrid, Y.; Gottlieb, H. E.; Marks, V.; Aurbach, D. *Electrochem. Solid-State Lett.* **2006**, *9*, A257.
- (5) Mizrahi, O.; Amir, N.; Pollak, E.; Chusid, O.; Marks, V.; Gottlieb, H.; Larush, L.; Zinigrad, E. *J. Electrochem. Soc.* **2008**, *155*, A103.
- (6) Vestfries, Y.; Chusid, O.; Goffer, Y.; Aped, P.; Aurbach, D. *Organometallics* **2007**, *26*, 3130.
- (7) Chen, C. R.; Gau, H. M. *Acta Crystallogr.* **2008**, *E64*, m1381.
- (8) Becke, A. D. *J. Chem. Phys.* **1993**, *98*, 5648–5652.
- (9) Lee, C.; Yang, W.; Parr, R. G. *Phys. Rev. B* **1988**, *37*, 785–789.
- (10) Hehre, W. J.; Radom, L.; Schleyer, P. v. R.; Pople, J. A. *Ab Initio Molecular Orbital Theory*; John Wiley & Sons: New York, 1986.
- (11) (a) Cance, M. T.; Mennucci, B.; Tomasi, J. *J. Chem. Phys.* **1997**, *107*, 3032. (b) Mennucci, B.; Tomasi, J. *J. Chem. Phys.* **1997**, *106*, 5151. (c) Mennucci, E.; Cancas, M. T.; Tomasi, J. *J. Phys. Chem. B* **1997**, *101*, 10506. (d) Tomasi, J.; Mennucci, B.; Cancas, E. *J. Mol. Struct. (THEOCHEM)* **1999**, *464*, 211.
- (12) Merrick, J. P.; Moran, D.; Radom, L. *J. Phys. Chem. A* **2007**, *111*, 11683.
- (13) Foster, J. P.; Weinhold, F. *J. Am. Chem. Soc.* **1980**, *102*, 7211–7218.
- (14) Frisch, M. J.; Trucks, G. W.; et al. Gaussian 09, revision A.02; Gaussian, Inc.: Wallingford, CT, 2009.
- (15) Nakayama, Y.; Kudo, Y.; Oki, H.; Yamamoto, K.; Kitajima, Y.; Noda, K. *J. Electrochem. Soc.* **2008**, *155* (10), A754.

- (16) (a) Ashby, E. C.; Parris, G. E. *J. Am. Chem. Soc.* **1971**, *93* (5), 1206. (b) Walker, F. W.; Ashby, E. C. *J. Am. Chem. Soc.* **1969**, *91* (4), 3845.
- (17) Shamir, J.; Sobota, P. *J. Raman Spectrosc.* **1991**, *22*, 535.
- (18) Jon, D. M.; Harker, Y. D.; David, F. E. *J. Chem. Phys.* **1969**, *50*, 5420.
- (19) Wotiz, J. H.; Hollingsworth, C. A.; Dessy, R. E. *J. Am. Chem. Soc.* **1956**, *78*, 1221.
- (20) Murakami, M.; Ue, A.; Nakamura, S. *J. Electrochem. Soc.* **2002**, *149*, A1572.
- (21) *Nonaqueous Electrochemistry*, Dekker, Inc.: New York, 1999.
- (22) Lee, J. Y.; Mhin, B. J.; Kim, K. S. *J. Phys. Chem. A* **2003**, *107* (19), 3578.
- (23) Bader, R. F. W.; Chang, C. *J. Phys. Chem.* **1989**, *93*, 2946.
- (24) Vigalok, A.; Milstein, D. *Acc. Chem. Res.* **2001**, *34*, 798.
- (25) Shaik, S.; Shurki, A.; Danovich, D.; Hiberty, P. C. *Chem. Rev.* **2001**, *101*, 1501.
- (26) Itzhaki, L.; Rozenal, E.; Altus, E.; Basch, H.; Hoz, S. *J. Phys. Chem. A* **2008**, *112* (50), 12812.